Journal of Solid State Chemistry 182 (2009) 1685–1690

Contents lists available at ScienceDirect

Journal of Solid State Chemistry

journal homepage: www.elsevier.com/locate/jssc

Synthesis, crystal structures, magnetic and luminescent properties of unique 1D *p*-ferrocenylbenzoate-bridged lanthanide complexes

P.F. Yan [a], F.M. Zhang [a], G.M. Li [a,*], J.W. Zhang [a], W.B. Sun [a], M. Suda [b], Y. Einaga [b]

[a] Key Laboratory of Functional Inorganic Material Chemistry (Heilongjiang University), Ministry of Education, School of Chemistry and Materials Science, Heilongjiang University, No. 74, Xuefu Road, Nangang District, Harbin 150080, PR China
[b] Keio University, 3-14-1 Hiyoshi, Yokohama 223-8522, Japan

ARTICLE INFO

Article history:
Received 25 July 2008
Received in revised form
2 January 2009
Accepted 15 January 2009
Available online 24 January 2009

Keywords:
Structures
P-ferrocenylbenzoate
Lanthanide
Luminescence
Magnetic property

ABSTRACT

Treatments of *p*-ferrocenylbenzoate [*p*-$NaOOCH_4C_6Fc$, Fc = (η^5-C_5H_5)Fe(η^5-C_5H_4)] with $Ln(NO_3)_3 \cdot nH_2O$ afford seven *p*-ferrocenylbenzoate lanthanide complexes $\{[Ln(OOCH_4C_6Fc)_2(\mu_2\text{-}OOCH_4C_6Fc)_2(H_2O)_2](H_3O)\}_n$ [*Ln* = Ce (**1**), Pr (**2**), Sm (**3**), Eu (**4**), Gd (**5**), Tb (**6**) and Dy (**7**)]. X-ray crystallographic analysis reveals that the isomorphous complexes $\{[Ce(OOCH_4C_6Fc)_2(\mu_2\text{-}OOCH_4C_6Fc)_2(H_2O)_2](H_3O)\}_n$ (**1**) and $\{[Pr(OOCH_4C_6Fc)_2(\mu_2\text{-}OOCH_4C_6Fc)_2(H_2O)_2](H_3O)\}_n$ (**2**) form a unique 1D double-bridged infinite chain structure bridged by μ_2-$OOCH_4C_6Fc$ groups. Each *Ln*(III) ion adopts a dodecahedron coordination environment with eight coordinated oxygen atoms from two terminal monodentate coordinated $FcC_6H_4COO^-$ units, two terminal monodentate coordinated H_2O molecules and four μ_2-$^-OOCH_4C_6Fc$ units. The luminescent spectra reveal that only **4** and **6** exhibit characteristic emissions of lanthanide ions, Eu(III) and Tb(III) ions, respectively. The variable-temperature magnetic properties of **5** and **7** suggest that a ferromagnetic coupling between spin carriers may exist in **5**.

1. Introduction

Carboxylate lanthanide complexes have been studied extensively in view of their structural diversity and physicochemical properties [1–11]. It is known that carboxylate usually adopt multiform binding modes such as terminal monodentate, chelating to one metal center, bridging bidentate in a syn–syn, syn–anti, anti–anti configuration to two metal centers, and bridging tridentate to two metal centers [12–14]. Moreover, almost all known carboxylate lanthanide complexes are coordination polymers. This may be attributed to the high coordination number and flexible coordination geometry of lanthanide ions. However, most of the previous documents have been focused on organic carboxylates such as oxalate, malonate, succinate, fumarate, maleate, terephthalate, and 1,3,5-benzenetricarboxylate. Organometallic carboxylate lanthanide complexes are rarely documented. As an important derivative of organometallic carboxylates, ferrocenecarboxylate has attracted much attention in coordination chemistry and magnetic properties in recent years [15–19]. Studies have revealed that ferrocenecarboxylate anions can act as terminal monodentate, bidentate and O,O-bridging ligands. A number of ferrocenecarboxylate transitional metal complexes have been reported [20–29]. Nevertheless, to our best knowledge, only three papers have been published on ferrocenecarboxylate lanthanide complexes. The first ferrocenecarboxylate lanthanide complex, $[Eu_2(Fcdc)_3(H_2O)_4]_n \cdot nH_2O$ (H_2Fcdc = 1,1′-ferrocenedicarboxylic acid) featuring a 2D interlinking zigzag-chain d-f mixed-metal network, was documented by Wong et al. in 2002 [18]. Hou et al. reported three ferrocenecarboxylato-bridged lanthanide dimmers $[Gd_2(\mu_2\text{-}OOCFc)_2(OOCFc)_4(MeOH)_2(H_2O)_2] \cdot 2MeOH \cdot 2H_2O$ (Fc = (η^5-C_5H_5)Fe(η^5-C_5H_4)), $[Nd_2(\mu_2\text{-}OOCFc)_2(OOCFc)_4(H_2O)_4] \cdot 2MeOH \cdot H_2O$, and $[Y_2(\mu_2\text{-}OOCFc)_2(OOCFc)_4(H_2O)_4] \cdot 2MeOH$ and their magnetic properties in 2003 [19]. Meng et al. revealed a 2D mixed-metal ferrocenyl-based coordination polymer, $[Sm_2L_3(H_2O)_5]$ (H_2L = 1,1′-ferrocenedicarboxylic acid), and studied its solid-state electrochemical property in 2003 [30]. It shall be noted that only 1,1′-ferrocenecarboxylate and 1-ferrocenedicarboxylate are found in the five known ferrocenecarboxylate lanthanide complexes. Other ferrocenecarboxylate lanthanide complexes are not documented. In view of versatile ferrocenecarboxylate ligands applied in transition metal complexes and the potential importance of the unique physicochemical properties of their lanthanide complexes, in this paper, a series of *p*-ferrocenylbenzoate lanthanide complexes with 1D chain structure are synthesized and described for the first time. Their magnetism and fluorescence have been examined and discussed.

* Corresponding author. Fax: +86 451 86604799.
E-mail addresses: gmli@hlju.edu.cn (G.M. Li), einaga@chem.keio.ac.jp (Y. Einaga).

0022-4596/$ - see front matter © 2009 Published by Elsevier Inc.
doi:10.1016/j.jssc.2009.01.015

2. Experimental section

2.1. General details

p-ferrocenylbenzoic acid and its sodium salt were prepared according to literature method [18]. $Ln(NO_3)_3 \cdot nH_2O$ were prepared by reactions of lanthanide oxide and nitric acid. All other chemicals were used as purchased. Elemental (C and H) analyses were performed on a Perkin-Elmer 2400 analyzer. IR spectra were conducted on Perkin-Elmer 60000 spectrophotometer with KBr pellets in the 400–4000 cm^{-1} region. UV–vis spectra were recorded on UV–2501 spectrophotometer in the range of 200–600 nm. Fluorescent spectra were taken on a LS-55 fluorescence photometer. Temperature-dependent magnetic susceptibility measurements on powder samples were conducted on a SQUID magnetometer (MPMS Quantum Design) over the temperature range 2–300 K. The magnetic field applied was 5000 Oe. The observed susceptibility data were corrected for underlying diamagnetism by using Pascal's constants. Diffraction intensity data for single crystal of complexes **1** and **2** were collected on a Rigaku R-AXIS RAPID imaging-plate X-ray diffractometer at 293 K. The structures were solved by the direct method and refined by the Full-matrix least squares on F^2 using the SHELXTL-97 software package [19]. All non-hydrogen atoms were refined anisotropically. Crystallographic data and important refinement parameters for **1** and **2** are summarized in Table 1.

Table 1
Crystallographic data and structure refinement for **1** and **2**.

	1	**2**
Empirical formula	$C_{68}H_{59}Fe_4O_{11}Ce$	$C_{68}H_{59}Fe_4O_{11}Pr$
Formula weight	1415.05	1416.46
Temperature (K)	293(2)	293(2)
Wavelength (Å)	0.71073	0.71073
Crystal system	Monoclinic	Monoclinic
Space group	*C*2/c	*C*2/c
a (Å)	44.863(9)	44.848(14)
b (Å)	14.714(3)	14.739(4)
c (Å)	10.474(2)	10.454(2)
α (°)	90	90
β (°)	97.43(3)	97.452(3)
γ (°)	90	90
V (Å^3)	6856(2)	6856(2)
Z	4	2
Calculated density (g/cm^3)	1.382	1.372
μ (mm^{-1})	1.532	1.578
F(000)	2880	2868
θ range for data collection (°)	3.14–27.48	3.14–27.45
Reflections collected/unique	32566/7778	32028/7802
R_{int}	0.1381	0.1246
R_1, wR_2 ($I>2\sigma(I)$)[a]	0.1007, 0.2870	0.0968, 0.2289
R_1, wR_2 (all data)[a]	0.1649, 0.2870	0.1518, 0.2610
Goodness-of-fit on F^2	0.948	1.043

[a] $R_1 = \Sigma||F_o|-|F_c||/\Sigma|F_o|$ and $wR_2 = \{\Sigma[w(F_o^2-F_c^2)^2]/\Sigma[w(F_o^2)^2]\}^{1/2}$.

2.2. Synthesis of $\{[Ln(OOCH_4C_6Fc)_2(\mu_2\text{-}OOCH_4C_6Fc)_2(H_2O)_2](H_3O)\}_n$ [Ln = Ce (**1**), Pr (**2**), Sm (**3**), Eu (**4**), Gd (**5**), Tb (**6**) and Dy (**7**)]

Complexes **1**–**7** were prepared in a similar manner as **1** (Scheme 1). A methanol solution (16 mL) of *p*-$NaOOCH_4C_6Fc$ (98.4 mg, 0.3 mmol) was layered on an aqueous solution (16 mL) of $Ce(NO_3)_3 \cdot 6H_2O$ (43.4 mg, 0.1 mmol) in a long tube. The tube was sealed and stored in darkness at ambient temperature. Complex **1** was gained and isolated in two weeks.

1, orange crystals, yield: 76.4 mg, 72%; Elementary anal. (%) Calc. for $C_{68}H_{59}Fe_4O_{11}Ce$ (1415.05): C, 57.66; H, 4.17. Found: C, 57.59; H, 4.14. IR (KBr, cm^{-1}): 3441 (m), 3083 (w), 1608 (s), 1574 (s), 1521 (s), 1395 (s), 1103 (w), 1002 (w), 793 (m), 705 (w), 478 (m). UV–vis (THF, nm): 253, 288.

2, orange crystals, yield: 74.4 mg, 70%; Elementary anal. (%) Calc. for $C_{68}H_{59}Fe_4O_{11}Pr$ (1416.46): C, 57.61; H, 4.16. Found: C, 57.63; H, 4.17. IR (KBr, cm^{-1}): 3434 (m), 3080 (w), 1604 (s), 1583 (s), 1513 (s), 1405 (s), 1181 (w), 1097 (w), 1004 (w), 795 (m), 710 (w), 478 (w). UV–Vis (THF, nm): 253, 288.

3, orange crystals, yield: 85.6 mg, 80%; Elementary anal. (%) Calc. for $C_{68}H_{59}Fe_4O_{11}Sm$ (1427.07): C, 57.18; H, 4.13. Found: C, 57.25; H, 4.20. IR (KBr, cm^{-1}): 3414 (m), 3083 (w), 1602 (s), 1574 (s), 1512 (s), 1409 (s), 782 (m), 472 (m). UV–vis (THF, nm): 255, 287.

4, orange crystals, yield: 83.5 mg, 78%; Elementary anal. (%) Calc. for $C_{68}H_{59}Fe_4O_{11}Eu$ (1428.07): C, 57.14; H, 4.13. Found: C, 57.26; H, 4.19. IR (KBr, cm^{-1}): 3390 (m), 3091 (m), 2962 (w), 1607 (s), 1578 (s), 1518 (s), 1404 (s), 1279 (w), 1182 (w), 1104 (m), 1080 (w), 1000 (w), 887 (w), 809 (m), 786 (s), 709 (m), 501 (m), 472 (s). UV–vis (THF, nm): 255, 287. Fluorescence spectrum (solid, nm): $\lambda_{ex} = 270$; $\lambda_{em} = 546, 592, 616, 650, 700$.

5, orange crystals, yield: 87.1 mg, 81%; Elementary anal. (%) Calc. for $C_{68}H_{59}Fe_4O_{11}Gd$ (1433.07): C, 56.94; H, 4.12. Found: C, 57.09; H, 4.07. IR (KBr, cm^{-1}): 3369 (w), 3089 (w), 1607 (s), 1581 (s), 1534 (s), 1423 (s), 118 (w), 1104 (m), 1000 (w), 888 (w), 808 (m), 786 (s), 707 (m), 503 (w), 473 (s). UV–Vis (THF, nm): 255, 289.

6, orange crystals, yield: 91.4 mg, 85%; Elementary anal. (%) Calc. for $C_{68}H_{59}Fe_4O_{11}Tb$ (1434.07): C, 56.90; H, 4.11. Found: C, 56.82; H, 4.19. IR (KBr, cm^{-1}): 3411 (w), 3089 (w), 1607 (s), 1581 (s), 1516 (s), 1414 (s), 1402 (s), 1281 (w), 1183 (w), 1105 (m), 1001 (w), 888 (w), 809 (m), 778 (s), 708 (m), 501 (w), 472 (s). UV–vis (THF, nm): 256, 287. Fluorescence spectrum (solid, nm): $\lambda_{ex} = 265$; $\lambda_{em} = 485, 558, 595$.

7, orange crystals, yield: 88.5 mg, 82%; Elementary anal. (%) Calc. for $C_{68}H_{59}Fe_4O_{11}Dy$ (1439.07): C, 56.70; H, 4.10. Found: C, 56.75; H, 4.10. IR (KBr, cm^{-1}): 3410 (w), 3089 (w), 2920 (m), 2850 (w), 1607 (s), 1582 (s), 1517 (s), 1421 (s), 1280 (w), 1181 (w), 1104

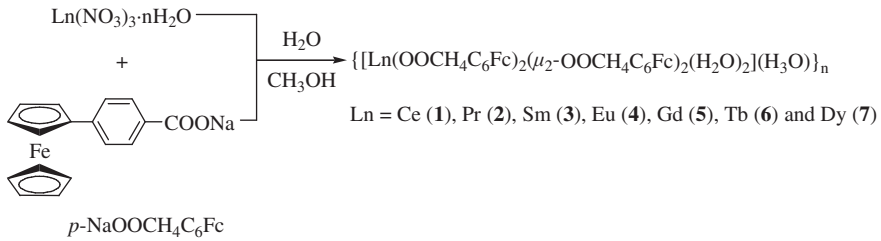

Scheme 1. Synthesis of **1**–**7**.

(w), 999 (w), 858 (w), 807 (m), 785 (s), 708 (m), 500 (w), 471 (s). UV–vis (THF, nm): 255, 288.

3. Results and discussion

3.1. Structural description of $\{[Ln(OOCH_4C_6Fc)_2(\mu_2\text{-}OOCH_4C_6Fc)_2(H_2O)_2](H_3O)\}_n$ [Ln = Ce (**1**), Pr (**2**)]

X-ray crystallographic analysis reveals that **1** and **2** are isomorphous crystallizing in the space group *C*2/c. In **1**, each Ce(III) ion is eight-coordinated by eight oxygen atoms in which two are from two water molecules, two are from two terminal monodentate coordinated $FcC_6H_4COO^-$ units and four are from four bidentate bridging μ_2-$FcC_6H_4COO^-$ groups, respectively (Fig. 1a). The ORTEP drawing with the atom labeling scheme of the coordination geometry of Ce(III) is depicted in Fig. 1b. In light of the dihedronal angle of 86.32° between two echelon planes of O2–$O2^i$–O4–$O4^i$ and $O3^{ii}$–$O3^{iii}$–$O5^i$–O5, which is close to the right angle, the coordinated Ce(III) ions are suggested to take the distorted triangle dodecahedron geometry. Obviously, two coordination modes for $FcC_6H_4COO^-$ are revealed, namely, terminal monodentate coordinated $FcC_6H_4COO^-$ and bidentate bridging μ_2-$FcC_6H_4COO^-$ groups. Although such two types of coordination modes are observed in ferrocenecarboxylate transition metal complexes $\{[Mn(OOCH_4C_6Fc)_2(\mu_2\text{-}OH_2)(H_2O)_2](H_2O)\}_n$ and $[Mn(\mu_2\text{-}OOCH_4C_6Fc)_2(phen)]_n$ (phen = 1,10-phenanthroline), respectively [31], they were not reported in their lanthanide analogues. Previously reported ferrocenecarboxylate ligand adopted bidentate chelating and tridentate μ-η^2:η^1-coordinating modes [18,19,30]. We suggest that the steric effect of the $FcC_6H_4COO^-$ group may dominate the differences. It is the bidentate bridging μ_2-$FcC_6H_4COO^-$ groups that connect the adjacent *Ln*(III) ions, forming a 1D double-bridged chain with the ferrocene moieties hanging on the two sides of these chain (Fig. 2). All phenylene rings in the complex are coplanar. The two neighboring phenylene rings are nearly perpendicular to each other. The dihedral angle between the two ring planes is 88.8°. The two corresponding phenylene rings are parallel to each other along the 1D chain. The dihedral angle between the two adjacent planes is 0°. The shortest distance between two parallel phenylene rings is 14.5 Å, which is too far away for efficient $\pi\cdots\pi$ interactions between two phenylene rings. Such a topology structure is somewhat similar to its transition metal analogue $[Mn(\mu_2\text{-}OOCH_4C_6Fc)_2(phen)]_n$ although the coordinating modes of $FcC_6H_4COO^-$ ligand are not the same. Nevertheless, it differs from the five known ferrocenecarboxylate lanthanide complexes, e.g. $[Eu_2(Fcdc)_3(H_2O)_4]_n \cdot nH_2O$ (H_2Fcdc = 1,1′-ferrocenedicarboxylic acid) exhibited a 2D interlinking zigzag-chain network [18], $[Gd_2(\mu_2\text{-}OOCFc)_2(OOCFc)_4(MeOH)_2(H_2O)_2]\cdot 2MeOH\cdot 2H_2O$, $[Nd_2(\mu_2\text{-}OOCFc)_2(OOCFc)_4(H_2O)_4]\cdot 2MeOH\cdot H_2O$ and $[Y_2(\mu_2\text{-}OOCFc)_2(OOCFc)_4(H_2O)_4]\cdot 2MeOH$ revealed the dimeric structures [19], $[Sm_2L_3(H_2O)_5]$ took a 2D mixed-metal ferrocenyl-based coordination polymer [30]. In **1**, the distances of Ce–O bonds are in the range of 2.407–2.601 Å (Table 2). The longest bond is the Ce–O

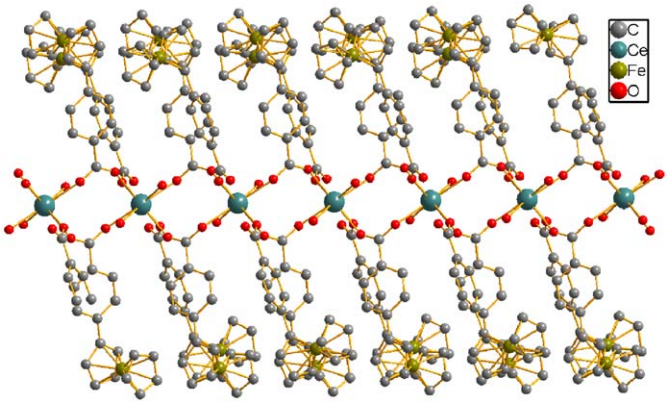

Fig. 2. 1D chain structure of **1** viewing along *b*-axis (hydrogen atoms and interstitial water molecules are omitted for clarity).

Table 2
Selected bond lengths (Å) and bond angles (°) of **1** and **2**.

1		**2**	
Ce1–O2	2.491(7)	Pr1–O2	2.497(7)
Ce1–$O3^{iii}$	2.416(6)	Pr1–$O3^{iii}$	2.389(7)
Ce1–O4	2.407(6)	Pr1–O4	2.382(6)
Ce1–O5	2.601(8)	Pr1–O5	2.560(8)
O2–Ce1–O5	129.3(3)	$O2^{ii}$–Pr1–O2	76.7(4)
$O2^i$–Ce1–O2	77.7(4)	$O2^{ii}$–Pr1–O5	129.4(3)
$O2^i$–Ce1–O5	128.9(3)	O2–Pr1–O5	129.2(3)
$O3^{ii}$–Ce1–O2	72.8(3)	$O3^{iii}$–Pr1–$O3^i$	146.9(4)
$O3^{ii}$–Ce1–$O2^i$	81.8(3)	$O3^i$–Pr1–O2	81.1(3)
$O3^{ii}$–Ce1–$O3^{iii}$	147.4(4)	$O3^i$–Pr1–$O2^{ii}$	73.0(3)
$O3^{ii}$–Ce1–O5	70.7(3)	$O3^i$–Pr1–O5	142.3(3)
$O3^{ii}$–Ce1–$O5^i$	141.8(3)	$O3^i$–Pr1–$O5^{ii}$	70.7(3)
O4–Ce1–O2	148.9(3)	$O4^{ii}$–Pr1–O4	140.5(4)
O4–Ce1–$O3^{ii}$	100.4(2)	O4–Pr1–O2	148.1(3)
O4–Ce1–$O3^{iii}$	90.7(2)	O4–Pr1–$O2^{ii}$	71.4(3)
O4–Ce1–$O4^i$	139.8(4)	O4–Pr1–$O3^i$	91.3(2)
O4–Ce1–O5	72.5(2)	O4–Pr1–$O3^{iii}$	99.8(2)
$O4^i$–Ce1–O2	71.3(3)	O4–Pr1–O5	73.1(3)
$O4^i$–Ce1–O5	75.2(3)	O4–Pr1–$O5^{ii}$	75.3(3)
$O5^i$–Ce1–O5	71.9(4)	$O5^{ii}$–Pr1–O5	72.2(4)

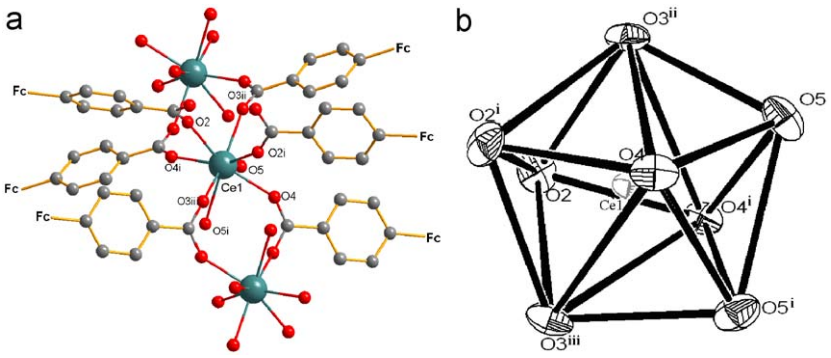

Fig. 1. (a) Crystal structure of **1** (hydrogen atoms, interstitial water molecules and ferrocenyl moieties are omitted for clarity); (b) Perspective view of the distorted triangle dodecahedron coordination geometry for Ce(III) ion in **1**.

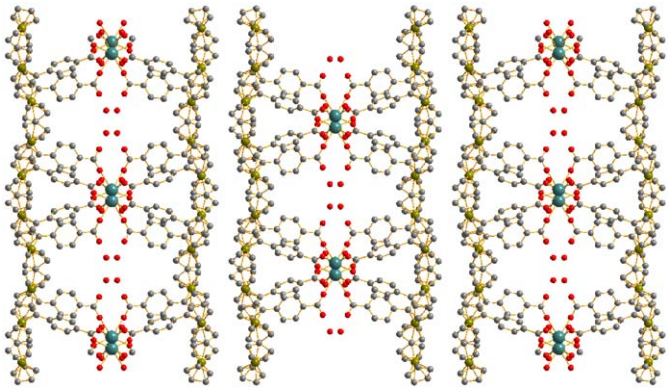

Fig. 3. Crystal packing structure of **1** or **2** viewing along *c*-axis.

(water) of 2.601(8) Å and the shortest bond is the Ce–O (bridging COO^-) of 2.407(6) Å. The bond distance of Ce–O (terminal COO^-) of 2.491(7) Å is in between. It suggests that the bonding sequence from strong to weak is the Ce–O (bridging COO^-), Ce–O (terminal COO^-) and the Ce–O (water) bonds. The average bond distance of Ce–O is 2.504 Å. It is in aggreement with that in $\{Ce_2(FcCOO)_6\}$ [32]. The Ce···Ce distance of 5.358 Å in **1** is close to that in $\{Ce_2(FcCOO)_6\}$. In **2**, the tendency of bond distance for Pr–O is similar to that of **1**. The bond distances of Pr–O are in the range of 2.382–2.560 Å. The average bond distance is ca. 2.471 Å. It is similar to 2.436 Å (ave.) in $\{[Pr_2(L\text{-}Pro)_6(H_2O)_4](ClO_4)_6\}_n$ (L-Pro = L-Proline) [33]. The Pr···Pr distance is 5.341 Å. It is close to 5.323 Å in $\{[Pr_2(L\text{-}Pro)_6(H_2O)_4](ClO_4)_6\}_n$.

Crystal packing structure of **1** or **2** along the *c* axis (Fig. 3) reveals that all the well-separated infinite chains are parallel to each other and packed along the *c* direction. It is similar to that of $\{[Mn(OOCH_4C_6Fc)_2(\mu_2\text{-}OH_2)(H_2O)_2](H_2O)\}_n$ but differs from other ferrocenecarboxylato lanthanide analogues.

3.2. Luminescence

The excitation and emission spectra of **4** and **6** in solid state excited at 270 nm (Fig. 4 and 5) exhibit the characteristic emissions of Eu(III) and Tb(III) ions, respectively. For **4** five peaks are observed that are attributed to the leaps of $^5D_0 \rightarrow {}^7F_0$ (546 nm), $^5D_0 \rightarrow {}^7F_1$ (592 nm), $^5D_0 \rightarrow {}^7F_2$ (616 nm), $^5D_0 \rightarrow {}^7F_3$ (650 nm) and $^5D_0 \rightarrow {}^7F_4$ (700 nm) (Fig. 4). As the $^5D_0 \rightarrow {}^7F_0$ transition is relative weak, the spectrum reveals that Eu(III) in **4** occupies sites with low symmetry and without an inversion center, which is consistent with the crystal structures (Fig. 1b). The intensity of the $^5D_0 \rightarrow {}^7F_1$ transition, magnetic dipole transitions, depends only slightly on the environment of the Eu(III) center. However, the intensity of the $^5D_0 \rightarrow {}^7F_2$ transition, electric dipole transitions, is extremely sensitive to chemical bonds around Eu(III) ion, which increases as the site symmetry of the Eu(III) center decreases. Thus, the $I(^5D_0 \rightarrow {}^7F_2)/I(^5D_0 \rightarrow {}^7F_1)$ ratio is widely used as a criterion of the coordination state and site symmetry of the lanthanide ions. For **4**, the intensity ratio $I(^5D_0 \rightarrow {}^7F_2)/I(^5D_0 \rightarrow {}^7F_1)$ is equal to ca. **6**, which further indicates the low site symmetry of the Eu(III) ion. The intense $^5D_0 \rightarrow {}^7F_2$ transition suggests a highly polarizable chemical environment around the Eu(III) ion that is responsible for the red emission of **4**. It is similar to the characteristic emission of Eu(III) ion in several complexes, e.g. $\{[Eu_2(L)_3(H_2O)_3]\cdot 3H_2O\}_n$ (H_3L = 3,5-pyrazoledicarboxylic acid) [34], $[Eu_2(XA)_6(DMSO)_2]$ (HXA = xanthene-9-carboxylic acid; DMSO = dimethylsulfoxide) [35], $[Eu_5L_4(OH)_2(NO_3)_4(H_2O)_2]\cdot NO_3\cdot 3H_2O$, ($H_2L$ = *N,N′*-bis (5-bromo-3-methoxysalicylidene)phenylene-1,2-diamine) [36],

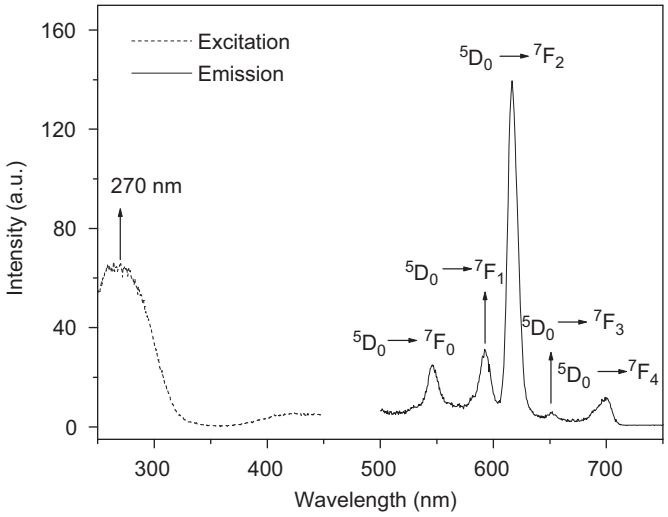

Fig. 4. Excitation and emission spectra of **4**.

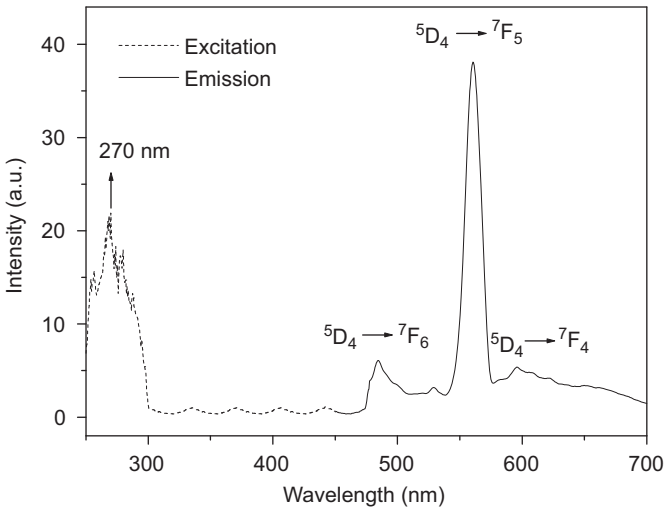

Fig. 5. Excitation and emission spectra of **6**.

$[EuCd(C_8H_7O_3)_5(phen)(H_2O)]$ ($C_8H_7O_3$ = 4-methoxybenzoato; phen = 1,10-phenanthroline) [37], $[L_3Eu_2]$ (L = chiral tartaric acid derived bis(*β*-diketonate) [38], $[Eu(tta)_3(Fc_2phen)]$ (tta = 2-thenoyltrifluoroacetonate; Fc_2phen = bis(ferrocenyl-ethynyl)-1,10-phenanthroline), $[Eu(fta)_3(phen)]$ (fta = ferrocenoyltrifluoroacetone; phen = 1,10-phenanthroline) [39] and $[Eu(H_2salen)_{1.5}(NO_3)_3]$ (H_2salen = *N,N′*-ethylenebis(salicylideneimine)) [40]. For **6**, three peaks are revealed at 485, 558 and 595 nm that are assigned to the transitions of $^5D_4 \rightarrow {}^7F_6$, $^5D_4 \rightarrow {}^7F_5$ and $^5D_4 \rightarrow {}^7F_4$, respectively (Fig. 5). However, the peak at 558 nm ($^5D_4 \rightarrow {}^7F_5$) is much stronger than other two bands. It is in agreement with the characteristic emission of Tb(III) ion in $[Tb_3(BDC)_{4.5}(DMF)_2(H_2O)_3\cdot(DMF)(H_2O)]$ (BDC = 1,4-benzenedicarboxylic acid; DMF = *N,N′*-dimethylformamide) [41], $\{[Tb_2(L)_3(H_2O)_3]\cdot 3H_2O\}_n$ [34], $[Tb_2(XA)_6(DMSO)_2]$ [35], $[TbCd(C_8H_7O_3)_5(phen)(H_2O)]$, $[Tb(H_2L)(NO_3)_3]$ (H_2L = *N,N′*-ethylene-bis(3-methoxysalicylideneimine)) [42], $[(H_2L)Tb(NO_3)_3]$ (H_2L = *N,N′*-bis(2-hydroxy-3-methoxybenzylidene)-N-ethylic-1,2-dimine) [43] and $[Tb_2(3,4\text{-}pyda)_3(phen)(H_2O)\cdot H_2O]_n$ (3,4-pyda = pyridine-3,4-dicarboxylic acid) [44]. Noticeably, the transition intensity of **4** is three times stronger than that of **6**. It means that the energy transfer from the organic ligand to Eu(III) ion is more effective than that to Tb(III)

ion. Since the characteristic emissions of corresponding Sm(III) and Dy(III) ions of **3** and **7** were not observed, the energy transfer from the *p*-ferrocenylbenzoic ligand to Sm(III) and Dy(III) ions is inefficient according to the theory of energy transfer [45,46].

3.3. Magnetism

The variable-temperature magnetic susceptibility measurements of **5** and **7** were performed in the temperature range of 2–300 K at 5000 Oe field. Fig. 6 and 7 show the temperature dependence of the magnetic susceptibility of **5** and **7** in the forms of $\chi_m T$ vs T and χ_m^{-1} vs T, respectively. The value of $\chi_m T$ at 300 K for **5** is 8.13 emu mol^{-1} K which is close to the value for one free Gd(III) ion ($\chi_m T = 7.88$ emu mol^{-1} K, $g = 2$) [47]. When the temperature is decreased, the value of $\chi_m T$ increases up to a maximum of 8.46 emu mol^{-1} K at ca. 50 K and then abruptly decreases down to a minimum 7.25 emu mol^{-1} K at 2 K. The thermal evolution of χ_m^{-1} for **5** obeys the Curie–Weiss law, $\chi_m = C/(T-\theta)$, over the temperature range from 50 to 300 K with $C = 8.13$ emu mol^{-1} K and $\theta = 3.35$ K. All of these results suggest that a ferromagnetic coupling between Gd(III) ions exists in **5** although the Gd···Gd distance is long up to 5 Å in the 1D chain [48,49]. The carboxyl bridge may provide an effective interaction path for the ferromagnetic coupling.

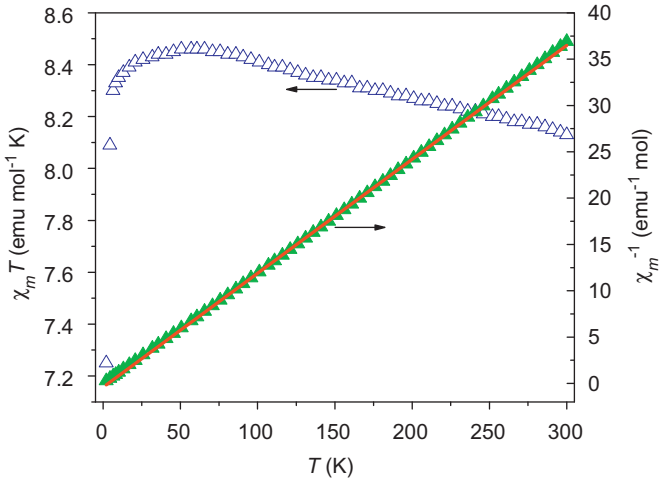

Fig. 6. Plots of $\chi_m T$ vs T and χ_m^{-1} vs T for **5**.

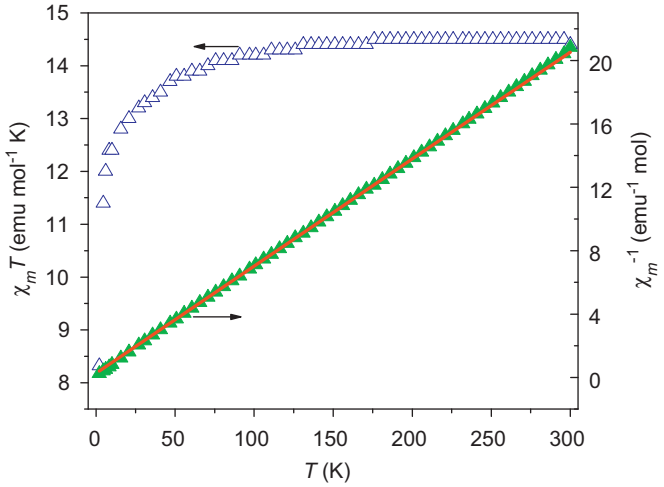

Fig. 7. Plots of $\chi_m T$ vs T and χ_m^{-1} vs T for **7**.

In contrast to **5**, it is very difficult to explain **7**'s magnetic properties because of the orbital contribution although they have the same structure. Usually, the spin-orbital coupling leads the $4f^n$ configuration of *Ln*(III) ions, except for Gd(III), to split into $^{2S+1}L_J$ states, and the latter further splits into Stark components under the crystal-field perturbation [50]. The $\chi_m T$ value of **7** at 300 K is 14.40 emu mol^{-1} K that is slightly higher than the value for one isolated Dy(III) ion ($\chi_m T = 14.17$ emu mol^{-1} K, $g = 4/3$) [47]. As the temperature is lowered, the $\chi_m T$ value decreases gradually and reaches 8.32 emu mol^{-1} K at 2 K. The thermal population of χ_m^{-1} for **7** is fit to the Curie–Weiss law, $\chi_m = C/(T-\theta)$, over the high temperature range with $C = 14.80$ emu mol^{-1} K and $\theta = -3.92$ K. The whole profile of the $\chi_m T$ versus T curve and the negative θ value should derive from the thermal depopulation of the Stark levels of Dy(III) ion and/or the antiferromagnetic coupling between Dy(III) ions through the carboxyl bridge, because these two magnetic behaviors all lead to the decrease of the $\chi_m T$ value with the cooling temperature [49,50].

4. Conclusion

Isolation and characterization of **1** and **2** demonstrate that *p*-ferrocenylbenzoate can stabilize lanthanide ions to form a unique 1D double bridge chain structure for the first time, in which $FcC_6H_4COO^-$ unit coordinated to the *Ln*(III) ion by two coordination modes. It differs from *p*-ferrocenylbenzoate transition metal complexes. These data together with previous literatures may provide important information on the design and synthesis of organometallic carboxylate lanthanide complexes. Various ferrocenylcarboxylate lanthanide complexes could be synthesized by using versatile ferrocenylcarboxylate ligands depending on the function need. Luminescence studied proposed that the *p*-ferrocenylbenzoate ligand exhibits a good antennae effect with respect to the Eu(III) and Tb(III) ions due to the ligand to metal energy transfer. Magnetic data suggest that ferromagnetic interactions appear in Gd(III) complex, however, the depopulation of Stark levels in Dy(III) complex dominates the magnetic properties in the whole temperature range. This approach of incorporating *p*-ferrocenylbenzoate group into lanthanide ions presents opportunities for the design of multifunctional materials.

Supplementary data

Crystallographic data (excluding structure factors) for the structure(s) reported in this paper have been deposited with the Cambridge Crystallographic Data Centre as supplementary publication no. CCDC 639697 and 639696 for **1** and **2**, respectively. Copies of the data can be obtained free of charge on application to CCDC, 12 Union Road, Cambridge CB2 1EZ, UK (fax: (44) 1223 336-033; e-mail: deposit@ccdc.cam.ac.uk).

CCDC Nos. contain the supplementary crystallographic data for this paper. These data can be obtained free of charge via http://www.ccdc.cam.ac.uk/conts/retrieving.html, or from the Cambridge Crystallographic Data Centre, 12 Union Road, Cambridge CB2 1EZ, UK; fax: (+44) 1223-336-033; or e-mail: deposit@ccdc.cam.ac.uk.

Acknowledgments

This work is financially supported by the National Natural Science Foundation of China (Nos. 20672032 & 20572018), Key Laboratory of Heilongjiang Province and Education Department of

Heilongjiang Province (nos. ZJG0504, JC200605, 1152GZD02 & 2006FRFLXG031).

Appendix A. Supplementary material

Supplementary data associated with this article can be found in the online version at 10.1016/j.jssc.2009.01.015.

References

[1] A. Ouchi, Y. Suzuki, Y. Ohki, Y. Koizumi, Coord. Chem. Rev. 92 (1988) 29 and references therein.
[2] T. Imai, M. Shimoi, A. Ouchi, Bull. Chem. Soc. Jpn. 60 (1987) 159 and references therein.
[3] J.F. Ma, Z.S. Jin, J.Z. Ni, Acta Chim. Sinica (Chin. Ed.) 51 (1993) 265.
[4] Y. Ohki, Y. Suzuki, T. Takeuchi, M. Shimoi, A. Ouchi, Bull. Chem. Soc. Jpn. 59 (1986) 1015.
[5] D.L. Zhang, C.H. Huang, G.X. Xu, Q.T. Zheng, C.H. He, Chinese J. Inorg. Chem. (Chin. Ed.) 8 (1992) 22.
[6] R. Vaidhyanathan, S. Natarajan, C.N.R. Rao, Chem. Mater. 13 (2001) 185.
[7] D.F. Sun, R. Cao, Y.C. Liang, Q. Shi, M.C. Hong, J. Chem. Soc., Dalton Trans. (2002) 1847.
[8] I. Georgieva, N. Trendafilova, A.J.A. Aquino, H. Lischka, Inorg. Chem. 46 (2007) 10926.
[9] L. Cañadillas-Delgado, O. Fabelo, J. Pasán, F.S. Delgado, M. Déniz, E. Sepúlveda, M.M. Laz, M. Julve, C. Ruiz-Pérez, Cryst. Growth Des. 8 (2008) 1313.
[10] R.S. Zhou, L. Ye, H. Ding, J.F. Song, X.Y. Xu, J.Q. Xu, J. Solid State Chem. 181 (2008) 567.
[11] Y.Q. Guo, S.F. Tang, B.P. Yang, J.G. Mao, J. Solid State Chem. 181 (2008) 2713.
[12] C. Policar, F. Lambert, M. Cesario, I. Morgenstern-Badarau, Eur. J. Inorg. Chem. (1999) 2201.
[13] F. Ribot, P. Toledano, C. Sanchez, Inorg. Chim. Acta 185 (1991) 239.
[14] J.M. Rueff, N. Masciocchi, P. Rabu, A. Sironi, A. Skoulios, Eur. J. Inorg. Chem. (2001) 2843.
[15] C. López, R. Costa, F. Illas, E. Molins, E. Espinosa, Inorg. Chem. 39 (2000) 4560.
[16] H. Hou, L. Li, G. Li, Y. Fan, Y. Zhu, Inorg. Chem. 42 (2003) 3501.
[17] G. Li, Y.L. Song, H.W. Hou, L.K. Li, Y.T. Fan, Y. Zhu, X.R. Meng, L.W. Mi, Inorg. Chem. 42 (2003) 913.
[18] Y.Y. Yang, W.T. Wong, Chem. Comm. (2002) 2716.
[19] H.W. Hou, G. Li, L.K. Li, Y. Zhu, X.R. Meng, Y.T. Fan, Inorg. Chem. 42 (2003) 428.
[20] A.L. Abuhijleh, C. Woods, J. Chem. Soc., Dalton Trans. (1992) 1249.
[21] S.D. Christie, S. Subramanian, L.K. Thompson, M.J. Zaworotko, Chem. Commun. (1994) 2563.
[22] S.M. Lee, K.K. Cheung, W.T. Wong, J. Organomet. Chem. 506 (1996) 77.
[23] N. Prokopuk, D.F. Shriver, Inorg. Chem. 36 (1997) 5609.
[24] F.A. Cotton, L.R. Fallvello, A.H. Reid, J.H. Tocher, J. Organomet. Chem. 319 (1987) 87.
[25] R. Costa, C. López, E. Molins, E. Espinosa, Inorg. Chem. 37 (1998) 5686.
[26] M.R. Churchill, Y.J. Li, D. Nalewajer, P.M. Schaber, J. Dorfman, Inorg. Chem. 24 (1985) 2684.
[27] R. Costa, C. López, E. Molins, E. Espinosa, J. Pérez, J. Chem. Soc., Dalton Trans. (2001) 2833.
[28] G. Li, B.Y. Chen, L.K. Li, J. Coord. Chem. 56 (2003) 877.
[29] M.W. Cooke, C.A. Murphy, T.S. Cameron, Inorg. Chem. Commun. 3 (2000) 721.
[30] D. Guo, B.G. Zhang, C.Y. Duan, X. Cao, Q.J. Meng, J. Chem. Soc., Dalton Trans. (2003) 282.
[31] H.W. Hou, L.K. Lin, Y. Zhu, Y.T. Fan, Y.Q. Qiao, Inorg. Chem. 43 (2004) 4767.
[32] L.L. Wen, B.G. Zhang, Z.H. Peng, J.G. Ren, C.Y. Duan, Chinese J. Inorg. Chem. (Chin. Ed.) 20 (2004) 1228.
[33] Z.L. Wang, C.J. Niu, N.H. Hu, J.Z. Ni, Acta Chim. Sinica (Chin. Ed.) 51 (1993) 257.
[34] J. Xia, B. Zhao, H.S. Wang, W. Shi, Y. Ma, H.B. Song, P. Cheng, D.Z. Liao, S.P. Yan, Inorg. Chem. 46 (2007) 3450.
[35] R. Shyni, S. Biju, M.L.P. Reddy, A.H. Cowley, M. Findlater, Inorg. Chem. 46 (2007) 11025.
[36] X.P. Yang, R.A. Jones, W.K. Wong, Dalton Trans. (2008) 1676.
[37] Y.X. Chi, S.Y. Niu, Z.L. Wang, J. Jin, Eur. J. Inorg. Chem. (2008) 2336.
[38] M. Albrecht, S. Schmid, S. Dehn, C. Wickleder, S. Zhang, A.P. Bassett, Z. Pikramenouc, R. Fröhlich, New J. Chem. 31 (2007) 1755.
[39] Y.F. Yuan, T. Cardinaels, K. Lunstroot, K. Van Hecke, L. Van Meervelt, C. Gorller-Walrand, K. Binnemans, P. Nockemann, Inorg. Chem. 46 (2007) 5302.
[40] T. Gao, P.F. Yan, G.M. Li, G.F. Hou, J.S. Gao, Polyhedron 26 (2007) 5382.
[41] X.D. Guo, G.S. Zhu, F.X. Sun, Z.Y. Li, X.J. Zhao, X.T. Li, H.C. Wang, S.L. Qiu, Inorg. Chem. 45 (2006) 2581.
[42] T. Gao, P.F. Yan, G.M. Li, G.F. Hou, J.S. Gao, Inorg. Chim. Acta 361 (2008) 2051.
[43] W. Dou, J.N. Yao, W.S. Liu, Y.W. Wang, J.R. Zheng, D.Q. Wang, Inorg. Chem. Commun. 10 (2007) 105.
[44] H.H. Song, Y.J. Li, Y. Song, Z.G. Han, F. Yang, J. Solid State Chem. 181 (2008) 1017.
[45] D.L. Dexter, J. Chem. Phys. 21 (1953) 836.
[46] T.D. Brown, T.M. Shcphcrd, J. Chem. Soc., Dalton Trans. (1973) 336.
[47] C. Benelli, D. Gatteschi, Chem. Rev. 102 (2002) 2369.
[48] Z. Zhang, Y. Song, T. Okamura, Y. Hasegawa, W. Sun, N. Ueyama, Inorg. Chem. 45 (2006) 2896.
[49] D. Weng, X. Zheng, X. Chen, L. Li, L. Jin, Eur. J. Inorg. Chem. (2007) 3410.
[50] J.P. Costes, F. Nicodème, Chem. Eur. J. 8 (2002) 3442.